On the Use of Generative Adversarial Networks to Predict Health Status Among Chronic Patients

María Teresa Jurado-Camino[1][a], David Chushig-Muzo[1][b], Cristina Soguero-Ruiz[1][c],
Pablo de Miguel Bohoyo[2][d] and Inmaculada Mora-Jiménez[1][e]

[1]*Dep. Signal Theory and Communications, Rey Juan Carlos University, Camino del Molino 5, Madrid, Spain*

[2]*University Hospital of Fuenlabrada, Madrid, Spain*

Keywords: Data Augmentation, Imbalance Learning, Decision Trees, Clinical Codes, Chronic Diseases.

Abstract: Chronic diseases (CD) are the leading cause of death worldwide, presenting higher mortality rates and economic burden (both in the health and social context) as the complexity of the CD increases. The use of Electronic Health Records (EHRs) and Machine Learning (ML) contribute to significant progress in health domain research, supporting identifying the patient's health status for early interventions. Despite these achievements, the class imbalance can limit the generalization capability of many ML models and data augmentation techniques are proposed to face this limitation. In this work, a Generative Adversarial Network named medWGAN is used to generate synthetic patients considering clinical data collected from EHRs linked to the University Hospital of Fuenlabrada. Data are associated with patients diagnosed with both simple CD (diabetes, hypertension, congestive heart failure, chronic obstructive pulmonary disease) and multiple CD. Experimental work using decision trees as predictors to determine the patient's health status showed the ability of medWGAN for preserving the underlying (high-dimensional and sparse) clinical patterns. Our results indicate that the identification of patients with multiple CD may benefit from the use of medWGAN as long as the data used for its training is diverse enough, contributing to supporting clinical decision-making in complex scenarios with many features.

1 INTRODUCTION

Several reports of the World Health Organization indicate that chronic diseases (CDs) are the leading cause of mortality worldwide, approximately reaching 71% of the total of deaths annually (Budreviciute et al., 2020). CDs are characterized by a gradual and slow progression, requiring a modification of the patient's lifestyle and continuous medical attention (Wagner and Brath, 2012). Among CDs, cardiovascular diseases, diabetes and lung diseases have become the most significant ones (Budreviciute et al., 2020) and health policies are seeking new strategies to tackle them (Wagner and Brath, 2012).

The extensive adoption of electronic health records (EHRs) has brought the opportunity to collect data and design data-driven models to support the early identification of patients at risk of suffering from CDs. In particular, Machine Learning (ML) approaches have received great attention in recent years to find hidden patterns in the data and extract knowledge from large and heterogeneous datasets (Shameer et al., 2018). Despite the great potential of ML, dealing with class imbalance (CI) (He and Garcia, 2009), which occurs when the number of instances is fairly uneven across classes, may limit the success of the resulting models. Since training of ML predictive models seeks to minimize an empirical loss function, learning is more focused on the samples of the majority class to the detriment of those in the minority classes (He and Garcia, 2009).

Handling CI is a challenge in many practical applications, with the health domain being one of the most outstanding, since patients in the minority classes deserve special attention from a clinical viewpoint. To tackle the CI problem, two main paradigms are usually considered to construct a balanced dataset (Ma and He, 2013). The first one con-

[a] https://orcid.org/0000-0002-5646-1290
[b] https://orcid.org/0000-0001-5585-2305
[c] https://orcid.org/0000-0001-5817-989X
[d] https://orcid.org/0000-0001-5241-596X
[e] https://orcid.org/0000-0003-0735-367X

Jurado-Camino, M., Chushig-Muzo, D., Soguero-Ruiz, C., Bohoyo, P. and Mora-Jiménez, I.
On the Use of Generative Adversarial Networks to Predict Health Status Among Chronic Patients.
DOI: 10.5220/0011690500003414
In *Proceedings of the 16th International Joint Conference on Biomedical Engineering Systems and Technologies (BIOSTEC 2023) - Volume 5: HEALTHINF*, pages 167-178
ISBN: 978-989-758-631-6; ISSN: 2184-4305

siders undersampling methods, based on keeping all samples from the minority class and discarding samples from the majority class. The main drawback of using the undersampling paradigm is that the number of samples (especially in the health domain) is usually quite reduced, and it is not convenient to lose some of them. To avoid discarding samples, the oversampling paradigm (He and Garcia, 2009) generates new (synthetic) samples for the minority classes. In this line, the Synthetic Minority Oversampling Technique (SMOTE) (Chawla et al., 2002) is one of the most used approaches because of its simplicity, since it is based on a linear interpolation of samples in the minority classes. Nevertheless, SMOTE does not work properly with categorical features, since the distance calculation and interpolation become challenging (Engelmann and Lessmann, 2021). In this scenario, the techniques based on Generative Adversarial Networks (GANs) emerge as a promising approach to generate synthetic data, often improving the model's performance in classification tasks and additionally mitigating data privacy concerns (Creswell et al., 2018). GANs have attracted attention both in academia and industry due to their remarkable performance when creating numerical data, specifically in the computer vision field (Cao et al., 2018). However, their use for discrete and tabular data is still limited (Zhang et al., 2020) and specific architectures such as medWGAN (Baowaly et al., 2019) have been proposed in the medical industry.

This paper studies the use of synthesized data using GAN-based models, specifically medWGAN, to improve the generalization capabilities of nonparametric predictive models in complex scenarios with binary data. Specifically, we deal with a very limited number of samples characterized by a high number of binary features in a multi-class task. The study, which considers real-world records associated with chronic patients of the University Hospital of Fuenlabrada (UHF) in Spain has been approved by the Ethics Committee. To sum up, our work presents two main contributions: *(i)* analyze augmented realistic data using GAN-based models, applied to chronic populations (including multimorbidity) and using both diagnosis and drug codes; and *(ii)* to analyze and assess the performance of prediction models for CDs when designed just with real patient data and when incorporating synthetic ones.

The rest of the paper is organized as follows. Section 2 refers to the dataset description and the exploratory analysis. The ML methods considered in this work, both for generating synthetic patient data and for predictive analysis are shown in Section 3. Section 4 details the experimental setup for generation and evaluation of the synthetic samples. The predictive results for a multi-class scenario (including complex health statuses) considering both real data and a mixture of real and synthetic data in the model design are presented in Section 5. Finally, the main conclusions are shown in Section 6.

2 DATASET DESCRIPTION AND EXPLORATORY ANALYSIS

Information about age, gender, and clinical data (diagnoses and drugs) were extracted from EHRs of the UHF, linked to chronic patients with simple and multiple CDs. Diagnoses were coded according to the International Classification of Diseases, 9th Revision, Clinical Modification (ICD9-CM) (American Medical Association, 2004). Data associated with drugs followed the Anatomical Therapeutic Chemical (ATC) Classification System (World Health Organization, 2006). The use of ICD9-CM and ATC codes has been widely validated in many studies (Soguero-Ruiz et al., 2020a), (Bouza et al., 2016), (Falhammar et al., 2019).

Both ICD9-CM and ATC codes are composed of a fixed number of alpha-numeric characters (ANCs) hierarchically organized. The ICD9-CM codes have from three to five ANCs, with a decimal point between the third and fourth ANC. The ATC codes are identified by seven ANCs, structured in five levels: (1) anatomical (first ANC), (2) therapeutic (second-third ANCs), (3) pharmacological (fourth ANC), (4) chemical (fifth ANC), and (5) chemical substance (sixth-seventh ANCs). Similarly to prior works (Chushig-Muzo et al., 2021), (Soguero-Ruiz et al., 2020a), we reduced the detail of the clinical codes by discarding the ANC after the decimal point for ICD9-CM and the fifth level for ATC codes. Hence, each patient is represented by 2263 binary features, corresponding to 1517 ICD9-CM and 746 ATC codes. Each binary feature indicates the presence/absence of the corresponding code.

The population classification system named Clinical Risk Groups (CRGs) (Hughes et al., 2004), internationally validated by the healthcare community in different works (Finison et al., 2017), (Chong et al., 2019), (Chushig-Muzo et al., 2022), has been used to identify chronic patients. The CRG system consider data of patient encounters with the health system (age, gender, diagnoses, and pharmacological drugs) for a limited period (usually one year) and assign every patient to just one group. The CRG system has a total of 1080 health conditions (groups), each one identified by a five-digit number. The first digit indicates the core health group, directly linked to CDs (including more than one simultaneous predominant condition). There are 9 core health groups: (1) healthy; (2) history of the significant acute disease; (3) single minor CD; (4) minor CDs in multiple organ systems; (5) significant CD; (6) significant CDs in multiple organ systems; (7) dominant CD in three or more organ systems; (8) dominant malignancy; and (9) catastrophic. The first four digits in the CRG number indicate the CRG health condition and are referred to as base-CRG. The last digit indicates the severity level.

In this paper, we considered CRGs encompassing patients with just one CD (core health group started with 5). In particular, we consider the CRG-5179 (Congestive Heart Failure, CHF), the CRG-5192 (hypertension, HT), and the CRG-5424 (diabetes, DIA). To extend our analysis, individuals suffering from co-occurring CDs have been also considered. Given the importance of Chronic Obstructive Pulmonary Disease (COPD) and associated morbidities, we also included it in this study, though there is no CRG group identifying COPD as a single significant CD. Specifically, the examined CRGs with two co-occurring CDs (those starting with the number 6) were CRG-6190 (CHF and COPD), CRG-6191 (CHF and DIA), CRG-6313 (DIA and HT). Patients with co-occurring three CDs have also been considered (core health status started with 7), specifically CRG-7060 (CHF, DIA, and COPD), CRG-7080 (CHF, DIA, and another CD) and CRG-7081 (CHF, COPD, and another CD). It is worth noting that the third CD considered in CRG-7080 and CRG-7081 is not specified, with a potentially wide range of CDs in the same base-CRG.

A summary of some statistics for each CRG is shown in Table 1, with the number linked to the severity level indicated in the first column (between brackets). Although demographic variables (gender and age) are available, these were only used for characterizing CRGs and were not used for data augmentation or prediction purposes. Interestingly, note that as the first digit of the CRG (core health status) increases, the number of patients decreases, and the average age increases. Due to the high imbalance in the number of patients per base-CRG, we analyze the number of patients per severity level (four possible severity levels) for the CRG-5192, CRG-5424, and CRG-6313, which are the base-CRGs with the highest number of patients. We checked: *(i)* the imbalance in the size of the CRGs when considering the severity level; and *(ii)* the results obtained by training two GANs per base-CRG (one for generating synthetic samples with severity level 1, and the another one for generating samples with severity levels 2, 3 and 4).

Table 1: Statistics of the considered base-CRG (first column, with severity level in brackets): number of patients, # women, and age (mean±std).

base-CRG	# patients	% women	age (mean ± std)
5179	141	31.2	68.7 ± 14.2
5192(1)	7761	47.7	55.6 ± 12.0
5192(2)	1424	54.0	56.5 ± 11.2
5192(3)	100	39.0	60.1 ± 12.1
5192(4)	39	33.3	54.6 ± 9.6
5424(1)	1160	33.1	52.1 ± 12.0
5424(2)	506	36.4	40.9 ± 18.8
5424(3)	38	50.0	41.9 ± 20.4
5424(4)	5	20.0	48.4 ± 16.4
6190	102	54.9	77.7 ± 11.8
6191	131	32.8	71.7 ± 11.2
6313(1)	2123	36.9	60.5 ± 10.5
6313(2)	1337	42.7	62.4 ± 11.1
6313(3)	287	63.0	62.7 ± 11.1
6313(4)	55	58.2	62.9 ± 10.4
7060	159	57.9	75.4 ± 11.1
7080	99	61.6	72.7 ± 12.3
7081	188	49.0	79.2 ± 11.8

To gain knowledge of the most prevalent clinical codes associated with each CRG, we obtain the corresponding diagnosis and drug profile (Soguero-Ruiz et al., 2020a), (Chushig-Muzo et al., 2021). Since several CRGs are considered in this work, just the profiles of some base-CRGs not previously analyzed in the author's contributions are shown in this paper. In this line, the diagnosis/drug profile for CRG-5179, CRG-6191, CRG-7060 are presented on the left panels of Figure 1. The diagnosis profile of CRG-5179 (see Figure 1 (a)) shows that the ICD9-CM codes with the highest presence rate are 427 (cardiac dysrhythmias) and 428 (heart failure), which are closely related to CHF. Note that the present rate of codes 427 and 428 do not exceed 54% (see Table 2), showing that approximately half of the patients in CRG-5179 have not been diagnosed with these codes. It is also interesting that the 401 code (Essential Hypertension, EHT) presents a rate even higher than that linked to code 427, evidencing the relationship between these CDs (HT and CHF). The drug profile (see Figure 1 (c)) shows that patients in CRG-5179 mainly consume C03CA (sulfonamides), A02BC (proton pump inhibitors), and N02BE (anilides). The code C03CA corresponds to loop diuretics used for primarily treating uncompensated heart failure, A02BC is usually prescribed as a stomach protector, and N02BE are non-opioid analgesic. Regarding the diagnosis profile of CRG-6191 (see Figure 1 (e)), the ICD9-CM codes with the highest presence rate were 250 (DM), 401 (EHT), 427, and 428. The drug profile of CRG-6191 (see Figure 1 (g)) indicates that ATC codes most prevalent are C03CA, A02BC, N02BE and C10AA (HMG CoA reductase inhibitors). C10AA is commonly used for reducing high cholesterol levels and the other drugs were previously detailed. For CRG-7060 (CHF, DIA, and COPD), in the diagnosis profile (see Figure 1 (i)) the most frequent ICD9-CM codes were 250 (DM), 427, 428 (related to CHF), and 518 (linked to COPD), while the drug profile (see Figure 1 (k)) showed a high presence rate of ATC codes C03CA, A02BC, N02BE, and C10AA. A summary of the most frequent codes in the profiles for the rest of the considered CRGs is provided in Table 2.

Table 2: Most prevalent ICD9-CM codes in the base-CRGs, and associated presence rate. Values over 0.8 are in bold.

	ICD9-CM codes						
base-CRG	250	272	401	427	428	518	780
5179	0.03	0.21	0.47	0.4	0.54	0.04	0.18
5192(1)	0.01	0.22	0.79	0.01	0.00	0.00	0.08
5192(2)	0.01	0.25	**0.83**	0.01	0.00	0.00	0.16
5192(3)	0.01	0.42	**0.85**	0.01	0.00	0.03	0.18
5192(4)	0.00	0.33	**0.92**	0.00	0.00	0.00	0.13
5424(1)	**0.88**	0.22	0.05	0.00	0.00	0.00	0.07
5424(2)	**0.97**	0.15	0.04	0.00	0.00	0.00	0.01
5424(3)	**0.92**	0.26	0.08	0.00	0.00	0.00	0.13
5424(4)	**1.00**	0.20	0.00	0.00	0.00	0.00	0.00
6190	**0.91**	0.00	0.00	**0.93**	0.52	**0.80**	0.64
6191	**0.89**	0.31	0.64	0.45	0.54	0.07	0.23
6313(1)	**0.86**	0.25	0.69	0.01	0.00	0.00	0.17
6313(2)	**0.93**	0.31	0.73	0.02	0.00	0.00	0.22
6313(3)	**0.95**	0.37	0.79	0.01	0.00	0.00	0.28
6313(4)	**0.95**	0.38	**0.87**	0.04	0.02	0.09	0.31
7060	**0.89**	0.47	0.66	0.54	0.79	0.50	0.25
7080	**0.93**	0.48	0.67	0.32	0.69	0.26	0.34
7081	0.22	0.35	0.54	0.59	**0.87**	0.65	0.25

Table 3: Most prevalent ATC codes in the base-CRGs, and associated presence rate. Values over 0.8 are in bold.

	ATC codes							
base-CRG	A02BC	A10AB	A10BA	C03CA	C09AA	C10AA	N02BE	R03AC
5179	0.62	0.00	0.00	0.79	0.45	0.46	0.60	0.05
5192(1)	0.29	0.00	0.00	0.03	0.42	0.31	0.32	0.02
5192(2)	0.46	0.00	0.00	0.04	0.40	0.36	0.44	0.03
5192(3)	0.54	0.00	0.00	0.06	0.44	0.44	0.58	0.05
5192(4)	0.36	0.00	0.00	0.00	0.44	0.31	0.38	0.03
5424(1)	0.22	0.09	0.65	0.00	0.00	0.45	0.24	0.01
5424(2)	0.19	0.46	0.36	0.00	0.01	0.34	0.31	0.02
5424(3)	0.32	0.39	0.50	0.00	0.00	0.34	0.26	0.03
5424(4)	0.20	0.20	0.40	0.00	0.00	0.60	0.60	0.00
6190	**0.91**	0.00	0.00	**0.93**	0.53	0.52	**0.80**	0.64
6191	**0.80**	0.19	0.50	**0.93**	0.54	0.71	0.73	0.05
6313(1)	0.40	0.05	0.71	0.05	0.47	0.66	0.33	0.02
6313(2)	0.59	0.06	0.63	0.06	0.42	0.67	0.51	0.0
6313(3)	0.69	0.08	0.59	0.1	0.41	0.67	0.65	0.06
6313(4)	0.78	0.13	0.56	0.15	0.47	0.65	0.73	0.11
7060	**0.92**	0.46	0.38	**0.97**	0.53	0.64	**0.87**	0.72
7080	**0.88**	0.36	0.35	**0.94**	0.52	0.64	0.79	0.37
7081	**0.97**	0.14	0.09	**0.98**	0.54	0.42	**0.95**	0.66

For the CRG-5192, the ICD9-CM codes with the highest presence rate (see Table 2) were 401 (EHT) and 272 (disorders of lipid metabolism), showing the association between overweight and hypertension. Regarding the ATC codes, the highest presence rates are for drugs related to the cardiovascular system (see Table 2), with drugs like C09AA (ACE inhibitors) and C10AA. C09AA is the first-line drug recommended for treating hypertension, while C10AA is key for reducing cholesterol and preventing cardiovascular events. It is interesting to emphasize that the increase in the severity level is linked to an increase in the presence rate of non-steroidal anti-inflammatory medications (M01AE) and non-opioid analgesics (N02BE). For the CRG-5424, the diagnoses with the highest rate regardless of the severity level are 250 and 272, showing a link between DM and overweight. By analyzing the presence rate of the ATC codes in Table 3, A10BA (biguanides) and A10AB (insulins) were more frequent. Literature indicates that patients with type 1 diabetes require insulin therapy to maintain long-term glycemic control, while biguanides are antihyperglycemic agents used for type 2 diabetes (Raval and Vyas, 2020). Note also that the presence rate of insulin increases with the severity level of the base-CRG.

Concerning CRG-6190 (see Table 3), the ICD9-CM codes with the highest rate are 401 (EHT) and 427, 428 (linked to CHF). The drug codes with the highest presence rate are C03CA (loop diuretic, also frequent in patients of CRG-5179), and R03BB (anticholinergics, a medication for treating obstructive airway diseases). Regarding the CRG-6313, Table 2 shows high rates for the ICD9-CM codes 250 and 401. By analyzing ATC codes for CRG-6313 in Table 3, we observe a high presence rate of drugs for treating diabetes (A10BA) and cardiovascular diseases (C09AA and C10AA). When patients have more than CDs, more complex patterns in diagnoses and drugs can be identified. For the CRG-7080 (see Table 2), there is a high presence rate of ICD9-CM codes related to DM (250), CHF (428 or 427) and also 780 (general symptoms). Since the third chronic condition of patients encompassed in this CRG is not specified, there is a wide range of potential CDs. The ATC codes (see Table 3) with the highest rates are related to the cardiovascular system such as C03CA, C09AA, and C10AA and analgesics (N02BE).

Finally, for CRG-7081, the ICD9-CM codes with the highest rates are those related to EHT and CHF (401 and 427), and COPD and the respiratory system (518 and 519). There is also a high presence of antithrombotics (B01AB) and drugs related to the respiratory system (R01AX). In general, note that as the CRG number increases, the rate of A02BC, N02BE and M01AE also rises, showing that patients with co-occurrence of three CDs consume a high number of these drugs. Clinical evidence reveals that multimorbid patients generally consume multiple drugs for treating their diseases (Palmer et al., 2018) and consequently they require stomach protectors (ATC A02BC) to prevent any polypharmacy-related risks. Regarding analgesics, the literature indicates that their use increases with age (Roumie and Griffin, 2004), with 20-30% of older adults taking analgesic medication. Then, it seems reasonable to find these drug codes in CRGs with a predominant presence of elderly patients.

3 METHODS

The GAN-based methods for generating synthetic patient data are first described. Then, the model to predict the chronic health status of new patients, a decision tree (interpretable ML) is presented.

3.1 GAN-based Methods for Generating Patient Data

GANs are artificial neural networks designed to learn generative models through an adversarial process (Creswell et al., 2018). The GAN architecture is composed of two artificial networks: *(i)* a *generator G* that captures the distribution of the input data and generates synthetic samples by trying to mimic characteristics close similar to real data; and *(ii)* a *discriminator D* that tries to separate real from synthetic samples. Formally, G takes a random vector $\mathbf{z}$ from a distribution $F_z \sim \mathcal{N}(0,1)$ by creating a latent vector $\hat{\mathbf{x}}$. The generator D estimates the probability that input is taken from $\rho_{data}(x)$. Both G and D aim to optimize a zero-sum min-max game, with the value function $V(G,D)$ given by:

$$\min_{G} \max_{D} V(G,D) = \mathbb{E}_{x\sim\rho_{data}(x)}[\log D(\mathbf{x})] + \mathbb{E}_{z\sim\rho_{z}(z)}[\log(1-D(G(\mathbf{z})))], \qquad (1)$$

where $\rho_{data}(x)$ and $\rho_z(z)$ are the probability density function (pdfs) of real data and the noise (commonly uniform or spherical Gaussian distribution), and $\mathbb{E}[\cdot]$ is the symbol for the expectation.

GANs have been used in multiple applications, especially in computer vision for generating high-quality and trustworthy images (Cao et al., 2018). However, the conventional GAN was designed to learn the distribution of continuous values and it could not work properly with discrete data (Choi et al., 2017). The medGAN was proposed for handling high-dimensional binary and tabular data, and it was specifically trained with clinical codes extracted from EHRs (Choi et al., 2017). To work with binary data, the medGAN architecture (see Figure 2) introduces an autoencoder in the *generator* architecture to map discrete input samples to a continuous output, which is passed through the *decoder*. Despite the promising results of medGAN, it is prone to the *mode collapse* and the *mode drop*. In the former, the *generator* learns to map different inputs to the same output. In the second, the generator only captures certain regions of the underlying distribution of the real data. To stabilize GAN training and solve these challenges, several medGAN-like architectures have been proposed (Baowaly et al., 2019), introducing boundary-seeking GAN and Wasserstein GAN. Among these, medWGAN (Baowaly et al., 2019) improves the robustness and effectiveness for generating synthetic data with the addition of a weigh clipping called gradient penalty, changing the Jensen–Shannon divergence (original GAN) to the Wasserstein divergence. A schematic of the medWGAN procedure for training is shown in Figure 2. Note that the autoencoder has been trained as a prior step to performing medWGAN by taking as input real EHR data (high-dimensional binary feature vectors) and a fixed number of neurons in the latent space. According to (Baowaly et al., 2019), medWGAN outperforms other GAN architectures and works properly with binary features.

3.2 Interpretable Predictive Model for Multiclass Task

To identify chronic patients with different health statuses using just the presence of clinical codes, a decision tree (DT) has been considered (Bishop, 2006). It is a nonlinear and nonparametric technique providing a visual interpretation of how decisions are made in the predictions (Bishop, 2006). We have explored the use of DT in previous work with chronic conditions (Soguero-Ruiz et al., 2020b), showing good performance when considering high-dimensional binary clinical data. The underlying idea is to divide complex decisions into simpler ones, hierarchically organizing them with a tree-like shape, as indicated in Figure 3. When using a DT, the feature space is partitioned in an iterative manner into regions containing a more homogeneous set of observations. The root node is the beginning of the tree (see feature C03CA in Figure 3) and corresponds to the most important feature to solve the task. Each partition of the feature space is represented as an intermediate node below the root in the tree-like structure. The last nodes of the tree are called leaf nodes, and do not generate new partitions but assign a label to the encompassed

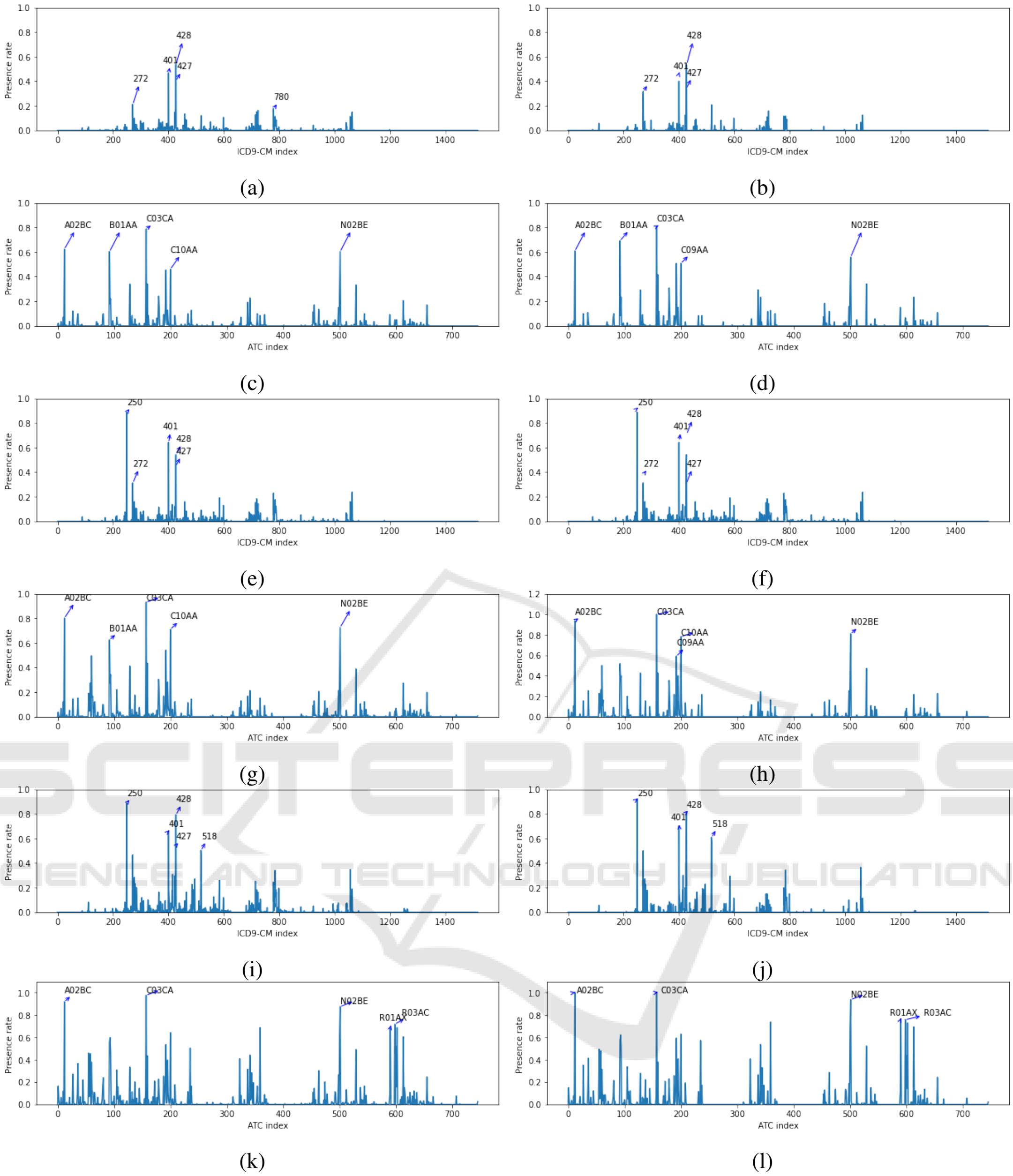

(a) (b) (c) (d) (e) (f) (g) (h) (i) (j) (k) (l)

Figure 1: Profiles with real samples (left panels) and synthetic samples (right panels): CRG 5179 (diagnosis profiles (a-b), drug profiles (c-d)); CRG 6191 (diagnosis profiles (e-f), drug profiles (g-h)); CRG 7060 (diagnosis profiles (i-j), drug profiles (k-l)).

samples.

We observe in Figure 3 that the code C03CA (drug related to the cardiovascular system) is the most relevant feature for identifying the chronic patients presented in Section 2. The presence rate shown in Table 2 for the ATC code C03CA is consistent with its presence on the root node: note that the leaf nodes shown in Figure 3 (absence of C03CA in the EHR) mostly correspond to the base-CRGs where C03CA has a low presence rate (CRG 5192, CRG 5424, and CRG 6313). When interpreting the rules in the DT, it is also important to consider the number of training samples on each leaf node. Specifically, the number of patients labeled by the DT in CRG 5179, CRG 6190, CRG 6191, and CRG 7060 (high presence rate for the code C03CA) is reduced (8, 4, 4, and 6). Despite the code C03CA being present in 93% of patients assigned to CRG 6190, the number of samples assigned to the leaf node shown in Figure 3 is low (4 out of 63, as detailed in Section 4), which corresponds

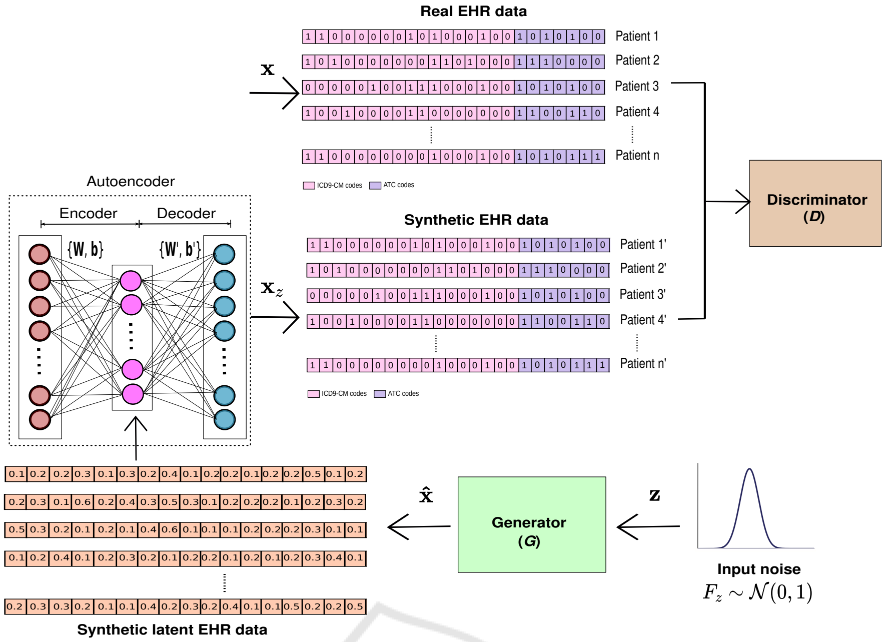
Real EHR data
1 1 0 0 0 0 0 0 1 0 1 0 0 0 1 0 0 1 0 1 0 1 0 0 Patient 1
1 0 1 0 0 0 0 0 0 0 1 1 0 1 0 0 0 1 1 1 0 0 0 0 Patient 2
0 0 0 0 0 1 0 0 1 1 1 0 0 0 1 0 0 1 0 1 0 1 0 0 Patient 3
1 0 0 1 0 0 0 0 1 1 0 0 0 0 0 0 0 1 1 0 0 1 1 0 Patient 4
1 1 0 0 0 0 0 0 0 0 1 0 0 0 1 0 0 1 0 1 0 1 1 1 Patient n
ICD9-CM codes
ATC codes
x
Autoencoder
Encoder
Decoder
{W, b}
{W', b'}
$\mathbf{x}_z$
Synthetic EHR data
1 1 0 0 0 0 0 0 1 0 1 0 0 0 1 0 0 1 0 1 0 1 0 0 Patient 1'
1 0 1 0 0 0 0 0 0 0 1 1 0 1 0 0 0 1 1 1 0 0 0 0 Patient 2'
0 0 0 0 0 1 0 0 1 1 1 0 0 0 1 0 0 1 0 1 0 1 0 0 Patient 3'
1 0 0 1 0 0 0 0 1 1 0 0 0 0 0 0 0 1 1 0 0 1 1 0 Patient 4'
1 1 0 0 0 0 0 0 0 0 1 0 0 0 1 0 0 1 0 1 0 1 1 1 Patient n'
ICD9-CM codes
ATC codes
Discriminator
(*D*)
0.1 0.2 0.2 0.3 0.1 0.3 0.2 0.4 0.1 0.2 0.2 0.1 0.2 0.2 0.5 0.1 0.2
0.2 0.3 0.1 0.6 0.2 0.4 0.3 0.5 0.3 0.1 0.2 0.2 0.2 0.1 0.2 0.3 0.2
0.5 0.3 0.2 0.1 0.2 0.1 0.4 0.6 0.1 0.1 0.1 0.2 0.2 0.2 0.3 0.1 0.1
0.1 0.2 0.4 0.1 0.2 0.3 0.2 0.1 0.2 0.2 0.1 0.2 0.1 0.2 0.3 0.4 0.1
0.2 0.3 0.3 0.2 0.1 0.1 0.4 0.2 0.3 0.2 0.4 0.1 0.1 0.5 0.2 0.2 0.5
Synthetic latent EHR data
$\hat{\mathbf{x}}$
Generator
(*G*)
$\mathbf{z}$
Input noise
$F_z \sim \mathcal{N}(0,1)$

Figure 2: Schematic of the medWGAN pipeline when considering high-dimensional binary feature vectors. This picture assumes the autoencoder has been previously trained taken as input real EHR data (feature vector **x**) by using a fixed number of neurons in the hidden layer.

to the 6% of the samples. It is interesting to remark that the branch number 0 in the DT (patients with the code C03CA, not shown in this paper for space issues) lead to the base-CRGs with 3 CDs, showing a presence rate above 94% for C03CA in Table 2.

Following branch number 1 in Figure 3, the next feature to be considered is code 250 (DM): if the code is not registered in the patient's EHR, branch number 2 is followed; otherwise, branch number 3. It is interesting to observe that the leaf node corresponding to CRG 5424 is located under the branch 3, showing that these patients have code 250 registered. This is consistent with the result shown in Table 2, where code 250 reaches a presence rate over 88% for CRG 5424. The next code to be considered is the diagnosis code 428 (related to CHF) for the branch number 2, and the code 401 (EHT) for branch number 3. The splitting procedure follows until reaching the leaf nodes, where the sample is assigned to a base-CRG. Note that the same feature (see the ICD9-CM 428, considered in branches 2 and 3) can be used in different parts of the DT.

When creating the DT by including an intermediate node with the attribute a, the homogeneity of the split is evaluated with the *Gini* impurity (Breiman et al., 2017) and optimizing the next cost function:

$$J(a,l_a) = \frac{m_{left}}{m} Gini_{left} + \frac{m_{right}}{m} Gini_{right} \qquad (2)$$

where a is the attribute chosen for the split, l_a is the threshold for the attribute, m is the total number of samples in the intermediate node, m_{left} is the number of samples sent to the left branch and m_{right} those sent to the right branch.

4 SYNTHETIC SAMPLES GENERATION AND EVALUATION

The real-world dataset was randomly split into the design and test subsets, with 80% and 20% of samples, respectively. The design subset is used for the synthetic sample generation, while the test subset is only used in Section 5 to evaluate the predictive models. We present in this section the experimental setup and the visual and quantitative results to evaluate the quality of synthetic data using the design subset.

4.1 Experimental Setup

The medWGAN was trained with the design subset for 200 epochs, experimentally checking it was enough for convergence when monitoring the validation loss (a validation subset was chosen for this purpose). The autoencoder architecture has 2263 neurons in the input and output layer, exploring three values (128, 64, and 32 neurons) for the size of the hidden

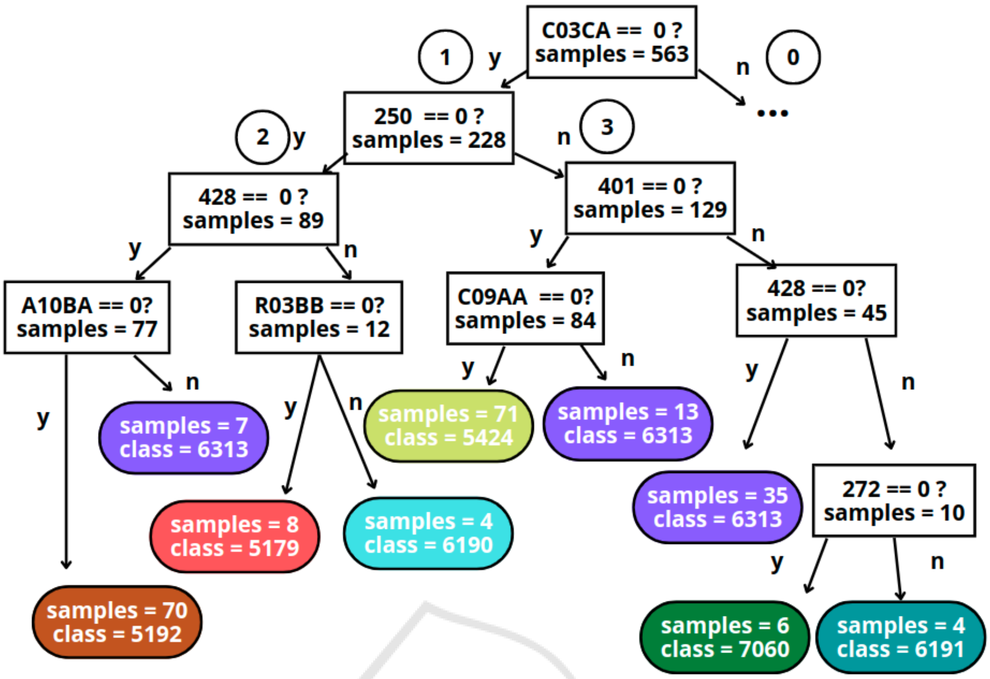

Figure 3: Detail of a branch of the DT using only the presence (arrow labelled as ‘n’) of diagnosis and drug codes to identify chronic patients in the considered CRGs.

layer (see Figure 2). The *generator G* is an artificial neural network, also exploring a different number of neurons in the layers {(128, 128), (64, 64), (32, 32)}. Regarding the *discriminator D*, it is also a neural network with 2263 neurons in the input layer and 1 neuron in the output layer. Three architectures with one hidden layer (32, 64 and 128 neurons) were explored for the *discriminator* network. Note that the number of neurons in the output of the *generator* matches with the number of neurons in the hidden layer of the autoencoder. As for number of neurons in the input layer of the *discriminator*, it is the same as the number of features in the input data. Following the same approach in prior works (Baowaly et al., 2019; Zhang et al., 2020), we selected the medWGAN architecture considering the *dimension-wise probability* (DWP), providing 64 neurons for both the *generator* and the *discriminator*.

To evaluate the quality of the generated synthetic samples from an ML perspective, we designed several decision trees, one DT per each base-CRG. For each one, we considered the same number of synthetic samples as those in the design subset (real-world samples). Since synthetic and real-world samples are joined in a new set called $\mathcal{X}_b$, every DT is built with balanced classes to discriminate between real-world and synthetic samples. The new set $\mathcal{X}_b$ was split into two partitions, one for the DT training (80%) and the other one for evaluation (20%).

The minimum number of samples per leaf was set to 10% of the number of training samples.

4.2 Visual and Quantitative Evaluation

In this subsection, a visual and quantitative comparison between the profiles obtained from real-world and synthetic patients is carried out. For the visual comparison, the diagnosis and drug profile of synthetic patients is obtained for each CRG. For simplicity, only the profiles of CRG-5179, 6191, and 7060 using synthetic data are depicted on the right panels of Figure 1. Note the high similarity between the profiles of real-world samples and those obtained from the synthetic samples (created with the medWGAN). As an example, note that the four ICD9-CM codes with the highest presence rates in CRG 5179 are the same when considering synthetic and real-world samples. It is also interesting to observe a regularization effect of the network since some codes with low presence rate when considering real-world samples have even a lower presence rates in the profile with the synthetic samples. To remark that, when the medWGAN considers a large number of real samples for training, the profiles created from real samples and synthetic samples are increasingly indistinguishable.

The first quantitative evaluation aims to measure the correlation between the profiles of real-world and synthetic data (Chushig-Muzo et al., 2022). Toward that end, the Pearson correlation coefficient (PCC) was considered. PCC is ranged between $[-1,1]$, with higher absolute values indicating high correlation and 0 meaning no linear relationship. Thus, we quantify the relationship between the profiles of real and synthetic patients corresponding to each CRG. High PCC values indicate that synthetic data is more similar to real data in terms of linear correlations across the features. The resulting PCC values for the profiles linked to all CRGs were over 0.9, showing that medWGAN captures reasonably well the characteristics of real-world data.

The second quantitative evaluation takes advantage of the potential of an ML classifier (specifically a DT) to determine whether samples are real-world or synthetic. Twelve DTs (one per CRG in Table 4) were designed for this purpose by considering just binary clinical codes. It is important to emphasize that, before the classifier design, a pre-processing stage is considered to ensure that every sample, real or synthetic, is unique. Details about the number of train and test samples (balanced classes), together with the accuracy rates in the test set are shown in Table 4. Note that results are fairly good, providing accuracy rates between 45%-66%.

Table 4: Accuracy in the test set when designing a DT for discriminating between real and synthetic samples (binary classification) linked to a specific CRG.

base-CRG	# train samples	# test samples	accuracy
5179	192	48	60.41%
5192(1)	8929	2233	54.23%
5192(234)	1584	386	54.29%
5424(1)	1433	359	52.36%
5424(234)	176	44	52.20%
6190	144	36	55.55%
6191	176	44	45.45%
6313(1)	1592	399	56.14%
6313(234)	1600	400	54.00%
7060	144	36	55.35%
7080	128	32	65.62%
7081	261	66	62.12%

5 HEALTH STATUS PREDICTION FOR CHRONIC PATIENTS

We now proceed to determine the patient's health status from a set of nine, all with chronic conditions. The nine health statuses correspond to the nine base-CRGs (5179, 5192, 5424, 6190, 6191, 6313, 7060, 7080, 7081) presented in Section 2, such that samples of all the severity levels linked to the same base-CRG are collected under the same base-CRG. To evaluate the performance in the multiclass scenario, the confusion matrix (CM) was used. For a scenario with 9 classes, the size of the CM is 9×9, showing the actual classes (rows in the CM) and the predicted ones (columns in the CM). Values in the entries in the diagonal cells report the number of samples with correct predictions, whereas those on the off-diagonal cells represent the number of misclassified samples.

Two settings are considered for learning: *(i)* the first setting, which uses just real-world data ($\mathcal{X}_r$); and *(ii)* the second setting, using both real-world and synthetic data ($\mathcal{X}_r \cup \mathcal{X}_s$). For both settings, a pre-processing stage is performed to ensure that any sample, real or synthetic, is unique and that the same sample (same feature vector) is not considered in different base-CRG. For a fair comparison, the model performance is always evaluated with real-world samples (test set), not considered neither to train the GANs and generate synthetic examples nor to train the DTs. For the multiclass DT, the validation set is obtained by randomly selecting 20% of the training set $\mathcal{X}_r$. Once the validation set is determined (note classes are unbalanced), we undersample the train set $\mathcal{X}_r$ for balancing purposes, leading to $\mathcal{X}_r'$, such that all the considered base-CRG have the number of samples of the base-CRG with fewer samples.

Several values for each hyperparameter were considered, selecting the model with the best performance following the multiclass Area Under the Curve (AUC) analysis (Hanley and McNeil, 1982) on the validation set. The AUC, a common figure of merit used in the clinical domain, reflects here how good the model is at identifying chronic patients with different health statuses. Since we are tackling a multiclass task, the AUC for each base-CRG is computed (see Table 5). To complement the results for multi-class classification, the macro average (macro-avg) and micro average (micro-avg) measurements were also calculated.

Once the model for the first setting has been designed (see part of the DT in Figure 3), we evaluate its performance using the test subset (only real-world samples). The corresponding CM is presented in Figure 4: the first value in every cell refers to the number of patients with the actual label (row) assigned to the predicted label (column); the second value is the first number expressed as a percentage (in relation to the actual label). The CM shows the worst performance for the base-CRG 7080 and 7081 (the chronic health statuses with more complex patterns). By analyzing the actual and predicted base-CRG, note that patients in the CRG 7081 are misclassified as the base-CRG 6190: both groups encompass patients with CHF and

Table 5: Multiclass AUC analysis on the validation subset, considering real samples ($\mathcal{X}'_r$) and five augmented sets ($\mathcal{X}'_r \cup \mathcal{X}_s$) composed by real and synthetic samples.

	$\mathcal{X}'_r$	$\mathcal{X}'_r \cup \mathcal{X}_s^{(1)}$	$\mathcal{X}'_r \cup \mathcal{X}_s^{(2)}$	$\mathcal{X}'_r \cup \mathcal{X}_s^{(3)}$	$\mathcal{X}'_r \cup \mathcal{X}_s^{(4)}$	$\mathcal{X}'_r \cup \mathcal{X}_s^{(5)}$
macro-avg	0.89	0.89	0.90	0.86	0.88	0.87
micro-avg	0.92	0.94	0.95	0.94	0.93	0.94
CRG-5179	0.94	0.94	0.97	0.97	0.95	1.00
CRG-5192	0.93	0.97	0.97	0.97	0.94	0.97
CRG-5424	0.87	0.89	0.90	0.86	0.91	0.87
CRG-6190	0.90	0.94	0.94	0.90	0.90	0.93
CRG-6191	0.90	0.85	0.83	0.83	0.83	0.78
CRG-6313	0.90	0.89	0.93	0.92	0.90	0.92
CRG-7060	0.92	0.88	0.80	0.78	0.82	0.80
CRG-7080	0.84	0.81	0.87	0.80	0.84	0.77
CRG-7081	0.77	0.85	0.87	0.72	0.80	0.78

COPD, though the base-CRG 7081 includes another unspecified pathology. In the same line, 9 patients assigned to the CRG 7080 are also misclassified in the CRG 6191, with both base-CRG sharing CHF and DM.

For the second setting using both real-world and synthetic data, we create five multiclass DTs with different subsets of synthetic samples. For this purpose, we randomly select five partitions from the $\mathcal{X}_s$ set, namely $\{\mathcal{X}_s^{(i)}\}_{i=1}^{5}$. Since the $\mathcal{X}_s$ set is unbalanced, we select the 90% of each base-CRG from $\mathcal{X}_s$ to obtain samples used in each partition. Then, we balance health statuses in each of the five partitions, obtaining 40 samples for each base-CRG and partition. To create each of the five multiclass DTs, we join the subset of real samples $\mathcal{X}'_r$ with each of other five subsets $\mathcal{X}_s^{(i)}$, such that $\{\mathcal{X}'_r \cup \mathcal{X}_s^{(i)}\}_{i=1}^{5}$ and design the five multiclass DTs. Finally, we obtain five CM linked to the same test set and the nine base-CRG. The average of the five CM is presented in Figure 5. It shows that the classification performance improves when including synthetic samples in the training set, especially for those health statuses with the lowest performance (multi-morbidity), which are more interesting from a clinical viewpoint.

6 CONCLUSIONS

In this work, we evaluated the use of medWGAN to generate synthetic clinical data aiming to improve the identification of chronic patients in a multi-class scenario. The medWGAN has resulted to be an effective method for creating synthetic feature vectors from high-dimensional clinical codes (ICD9-CM and ATC). To evaluate how similar synthetic and real-world patients are, the profiles and the PCC between profiles were first considered. The PCC values were over 0.9 in most cases, showing similar profiles and presence rates for the most prevalent

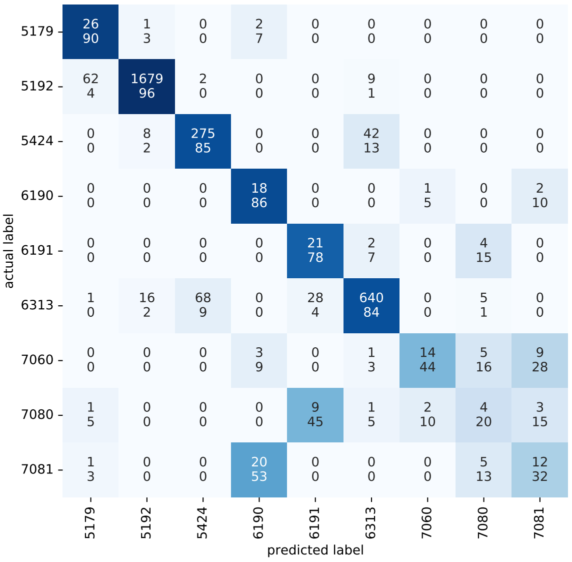

	5179	5192	5424	6190	6191	6313	7060	7080	7081
5179	26 90	1 3	0 0	2 7	0 0	0 0	0 0	0 0	0 0
5192	62 4	1679 96	2 0	0 0	0 0	9 1	0 0	0 0	0 0
5424	0 0	8 2	275 85	0 0	0 0	42 13	0 0	0 0	0 0
6190	0 0	0 0	0 0	18 86	0 0	0 0	1 5	0 0	2 10
6191	0 0	0 0	0 0	0 0	21 78	2 7	0 0	4 15	0 0
6313	1 0	16 2	68 9	0 0	28 4	640 84	0 0	5 1	0 0
7060	0 0	0 0	0 0	3 9	0 0	1 3	14 44	5 16	9 28
7080	1 5	0 0	0 0	0 0	9 45	1 5	2 10	4 20	3 15
7081	1 3	0 0	0 0	20 53	0 0	0 0	0 0	5 13	12 32

Figure 4: CM when evaluating the test subset (real-world samples) with the DT designed using only real-world samples (training samples). The first number in each cell refers to the number of patients with the actual label (rows in the CM) classified by the DT with the predicted label (columns in the CM). The second number in every cell represents the percentage of test patients of the actual class that are classified with different labels.

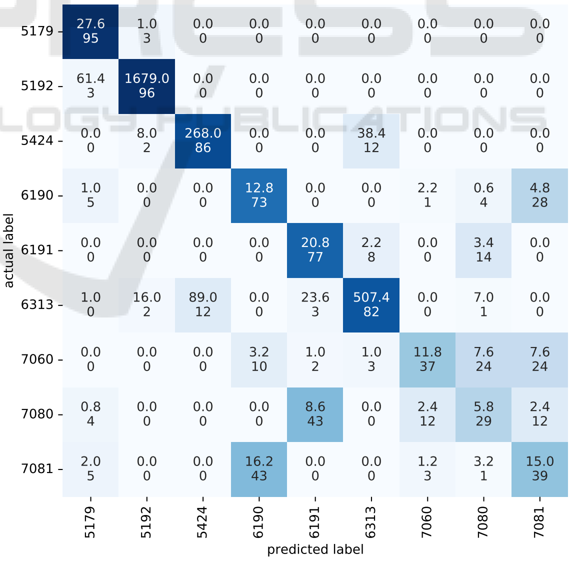

	5179	5192	5424	6190	6191	6313	7060	7080	7081
5179	27.6 95	1.0 3	0.0 0	0.0 0	0.0 0	0.0 0	0.0 0	0.0 0	0.0 0
5192	61.4 3	1679.0 96	0.0 0	0.0 0	0.0 0	0.0 0	0.0 0	0.0 0	0.0 0
5424	0.0 0	8.0 2	268.0 86	0.0 0	0.0 0	38.4 12	0.0 0	0.0 0	0.0 0
6190	1.0 5	0.0 0	0.0 0	12.8 73	0.0 0	0.0 0	2.2 1	0.6 4	4.8 28
6191	0.0 0	0.0 0	0.0 0	0.0 0	20.8 77	2.2 8	0.0 0	3.4 14	0.0 0
6313	1.0 0	16.0 2	89.0 12	0.0 0	23.6 3	507.4 82	0.0 0	7.0 1	0.0 0
7060	0.0 0	0.0 0	0.0 0	3.2 10	1.0 2	1.0 3	11.8 37	7.6 24	7.6 24
7080	0.8 4	0.0 0	0.0 0	0.0 0	8.6 43	0.0 0	2.4 12	5.8 29	2.4 12
7081	2.0 5	0.0 0	0.0 0	16.2 43	0.0 0	0.0 0	1.2 3	3.2 1	15.0 39

Figure 5: Averaged CM for the test subset (real-world samples) with the DT designed using real-world and augmented samples (training samples). Since five subsets of the synthetic samples were considered for training, the average of the five CM was computed. The first number in every cell refers to the average number of patients with the actual label (rows in the CM) classified by the DT with the predicted label (columns in the CM). The second number in each cell represents the average percentage of test patients of the actual class classified with different labels.

ICD9-CM and ATC codes. The classification results between real and synthetic samples also prove that these samples are hard to discriminate. Regarding the results in the multi-class scenario, the identification of patients with multiple chronic conditions was improved (specifically for patients assigned to CRG-6191, CRG-7080, and CRG-7081). Further research may explore cost-sensitive learning methods and GAN-based models that handle categorical and numerical features aiming to improve the classification results. Our study highlights the effectiveness of GAN-based models to work with a high-dimensional and sparse clinical dataset, allowing us to create realistic patient data and improve prediction performance.

ACKNOWLEDGMENT

This work was partly funded by the Spanish Research Agency, grant numbers PID2019-106623RB-C41/AEI/10.13039/501100011033 (BigTheory) and PID2019-107768RA-I00 (AAVis-BMR) funded by MCIN/AEI/10.13039/501100011033, by the Community of Madrid in the framework "Encouragement of Young Phd students investigation" (Mapping-UCI, F661), and by the European Union NextGenerationEU funds (Youth Employment Plan of the Spanish Government) in the INVESTIGO project with reference URJC-AI-11.

REFERENCES

American Medical Association (2004). International Classification of Diseases, 9th Revision, Clinical Modification.

Baowaly, M. K., Lin, C.-C., Liu, C.-L., and Chen, K.-T. (2019). Synthesizing electronic health records using improved generative adversarial networks. *Journal of the American Medical Informatics Association*, 26(3):228–241.

Bishop, C. M. (2006). *Pattern Recognition and Machine Learning (Information Science and Statistics)*. Springer-Verlag, Berlin, Heidelberg.

Bouza, C., Lopez-Cuadrado, T., and Amate-Blanco, J. (2016). Use of explicit ICD9-CM codes to identify adult severe sepsis: impacts on epidemiological estimates. *Critical Care*, 20(1):313.

Breiman, L., Friedman, J. H., Olshen, R. A., and Stone, C. J. (2017). *Classification and regression trees*. Routledge.

Budreviciute, A. et al. (2020). Management and prevention strategies for non-communicable diseases (ncds) and their risk factors. *Frontiers in Public Health*, 8:574111.

Cao, Y.-J., Jia, L.-L., Chen, Y.-X., Lin, N., Yang, C., Zhang, B., Liu, Z., Li, X.-X., and Dai, H.-H. (2018). Recent advances of generative adversarial networks in computer vision. *IEEE Access*, 7:14985–15006.

Chawla, N. V., Bowyer, K. W., Hall, L. O., and Kegelmeyer, W. P. (2002). Smote: synthetic minority oversampling technique. *Journal of Artificial Intelligence Research*, 16:321–357.

Choi, E., Biswal, S., Malin, B., Duke, J., Stewart, W. F., and Sun, J. (2017). Generating multi-label discrete patient records using generative adversarial networks. In *Proc of the Machine learning for Healthcare Conference*, pages 286–305, Boston, Massachusetts.

Chong, J. L., Lim, K. K., and Matchar, D. B. (2019). Population segmentation based on healthcare needs: a systematic review. *Systematic Reviews*, 8(1):1–11.

Chushig-Muzo, D., Soguero-Ruiz, C., de Miguel-Bohoyo, P., and Mora-Jiménez, I. (2021). Interpreting clinical latent representations using autoencoders and probabilistic models. *Artificial Intelligence in Medicine*, 122:102211.

Chushig-Muzo, D., Soguero-Ruiz, C., de Miguel-Bohoyo, P., and Mora-Jiménez, I. (2022). Interpreting clinical latent representations using autoencoders and probabilistic models. *BioData Mining*, 15(18):1–27.

Creswell, A., White, T., Dumoulin, V., Arulkumaran, K., Sengupta, B., and Bharath, A. A. (2018). Generative adversarial networks: An overview. *IEEE Signal Processing Magazine*, 35(1):53–65.

Engelmann, J. and Lessmann, S. (2021). Conditional wasserstein gan-based oversampling of tabular data for imbalanced learning. *Expert Systems with Applications*, 174:114582.

Falhammar, H., Lindh, J. D., Calissendorff, J., Skov, J., Nathanson, D., and Mannheimer, B. (2019). Antipsychotics and severe hyponatremia: A swedish population–based case–control study. *European Journal of Internal Medicine*, 60:71–77.

Finison, K., Mohlman, M., Jones, C., Pinette, M., Jorgenson, D., Kinner, A., Tremblay, T., and Gottlieb, D. (2017). Risk-adjustment methods for all-payer comparative performance reporting in vermont. *BMC Health Services Research*, 17(1):1–13.

Hanley, J. A. and McNeil, B. J. (1982). The meaning and use of the area under a receiver operating characteristic (roc) curve. *Radiology*, 143(1):29–36.

He, H. and Garcia, E. (2009). Learning from imbalanced data. *IEEE Transactions on Knowledge and Data Engineering*, 21(9):1263–1284.

Hughes, J. S., Averill, R. F., Eisenhandler, J., Goldfield, N. I., Muldoon, J., Neff, J. M., and Gay, J. C. (2004). Clinical Risk Groups (CRGs): a classification system for risk-adjusted capitation-based payment and health care management. *Medical Care*, 42(1):81–90.

Ma, Y. and He, H. (2013). *Imbalanced learning: foundations, algorithms, and applications*. John Wiley & Sons.

Palmer, K., Marengoni, A., Forjaz, M. J., Jureviciene, E., Laatikainen, et al. (2018). Multimorbidity care model: Recommendations from the consensus meeting of the joint action on chronic diseases and promoting healthy ageing across the life cycle (ja-chrodis). *Health Policy*, 122(1):4–11.

Raval, A. D. and Vyas, A. (2020). National trends in diabetes medication use in the united states: 2008 to 2015. *Journal of Pharmacy Practice*, 33(4):433–442.

Roumie, C. L. and Griffin, M. R. (2004). Over-the-counter analgesics in older adults. *Drugs & Aging*, 21(8):485–498.

Shameer, K., Johnson, K. W., Glicksberg, B. S., Dudley, J. T., and Sengupta, P. P. (2018). Machine learning in cardiovascular medicine: are we there yet? *Heart*, 104(14):1156–1164.

Soguero-Ruiz, C., Alonso-Arteaga, N., Muñoz-Romero, S., Rojo-Álvarez, J. L., Rubio-Sánchez, M., López-Fajardo, I. C., and Mora-Jiménez, I. (2020a). Finding associations among chronic conditions by bootstrap and multiple correspondence analysis. In *Intl Conf on Bioinformatics and Biomedicine*, pages 2066–2073, Seoul, Korea (South).

Soguero-Ruiz, C., Mora-Jiménez, I., Mohedano-Munoz, M. A., Rubio-Sanchez, M., Miguel-Bohoyo, P. d., and Sanchez, A. (2020b). Visually guided classification trees for analyzing chronic patients. *BMC Bioinformatics*, 21(2):1–19.

Wagner, K.-H. and Brath, H. (2012). A global view on the development of non communicable diseases. *Preventive Medicine*, 54:S38–S41.

World Health Organization (2006). The anatomical therapeutic chemical classification system with defined daily doses (ATC/DDD).

Zhang, Z., Yan, C., Mesa, D. A., Sun, J., and Malin, B. A. (2020). Ensuring electronic medical record simulation through better training, modeling, and evaluation. *J American Medical Informatics Association*, 27(1):99–108.